Materials and Design 90 (2016) 468–477

Contents lists available at ScienceDirect

Materials and Design

journal homepage: www.elsevier.com/locate/jmad



# Effect of bevel angle on microstructure and mechanical property of Al/steel butt joint using laser welding-brazing method

Junhao Sun [a,b,c], Qi Yan [a], Zhuguo Li [b,c], Jian Huang [a,b,c,*]

[a] State Key Laboratory of Development and Application Technology of Automotive Steels, 201900 Shanghai, China
[b] School of Materials Science and Engineering of Shanghai Jiao Tong University, 200240 Shanghai, China
[c] Shanghai key Laboratory of Materials Laser Processing and Modification, 200240 Shanghai, China

ARTICLE INFO

*Article history:*
Received 24 July 2015
Received in revised form 28 October 2015
Accepted 29 October 2015
Available online 31 October 2015

*Keywords:*
Al/steel butt joints
Fiber laser welding-brazing
Bevel angle
Microstructure
Tensile strength

ABSTRACT

Butt joining of AA6061 aluminum alloy and Q235 low-carbon steel of 2.5 mm thickness was conducted using laser welding-brazing method with ER4043 filler metal. An electro-galvanizing process of the steel was performed to obtain a zinc coating at the steel's bevel surface before welding. The brazing interface and the tensile strength of the joints were evaluated. The results showed that a sound butt joint between Al and steel was obtained, with the brazing interface consisted of zinc rich regions and a Fe–Al intermetallic (IMC) layer. The thickness and morphology of the IMC reaction layer were not constant but varied along the brazing interface. The morphology of the IMC reaction layer was more complex and the layer was thicker when a smaller bevel angle of the steel was used. All the joints fractured in the $Fe_2Al_5$ layer of the brazing interface. The tensile strength of the joints was mainly determined by the bonding area of the brazing interface, and average tensile strengths of 110 MPa and 150 MPa were achieved when bevel angles of 45° and 30° were used respectively.



## 1. Introduction

Hybrid structures of aluminum alloy and steel have been suggested to result in automobile lightweight structures and reduce fuel consumption [1,2]. Thus, it has become an attractive research field to join aluminum alloy and steel together in recent years. Producing reliable and cost effective dissimilar joints between them, hence, requires better metallurgical understanding of the joining techniques and their specific influence on the resulting microstructures [3].

The main issues associated with joining of aluminum to steel are the different physical properties between them (e.g. melting temperatures, thermal expansion and conductivity), the nearly zero solid solubility of Al in Fe and zero solid solubility of Fe in Al and the resulting formation of intermetallics [4]. According to L. Agudo [5], the formation of $Fe_xAl_y$ is necessary for achieving an effectual connection between the steel and Al. However, an excessive formation of $Fe_xAl_y$ IMCs, in particular of Al-rich $Fe_xAl_y$ IMCs (i. e., $Fe_2Al_5$, $FeAl_2$, $Fe_2Al_7$ and $FeAl_3$), results in the brittleness of the joints. Thus, the driving force for various welding techniques to join Al to steel is to minimize the thickness of brittle Al-rich IMC layer.

Many studies have been carried out to join Al and steel with both solid state and fusion based joining processes. In solid state joining process, such as friction stir welding [6,7,8], no IMC layer was formed along the Al/Fe interface or the formation of Fe–Al IMC was usually minimized, because there was basically only plastic deformation of the Al and the temperature generated during the joining process was very low (usually lower than the melting temperature of the substrate). Haddadi et al. [9] showed that Al to steel joint with high strength of 2.8 kN could be achieved using ultrasonic spot welding (USW), but their failure loads were limited by the formation of an interfacial reaction layer with excessive weld times. Self-piercing riveting (SPR) was used to join high-strength steel and aluminum alloy sheets in Ref. [10], and it was found the conventional SPR was effective in joining high-strength steel having a tensile strength below 590 MPa and aluminum alloy sheets in automobile parts. Friction bit joining (FBJ) method was also used to spot join aluminum alloy and dual phase 980 steel in Ref. [11], and optimized joint strength could be obtained by optimizing adhesive layer thickness. Explosion welding [12] had another advantage, as the process happened so quickly there was almost no time for the reaction between Fe and Al, thus the IMC layer formed during the process was also very thin. Song et al. [13] conducted TIG butt welding-brazing of 5A06 aluminum alloy and SUS321 stainless steel using 4047 AlSi12 filler metal. Results indicated that the joint reached an average tensile strength of 120 MPa, and fractured at the unequal interfacial layer which was ranged from 5 μm to 35 μm at different position of the joint; Dong et al. [14,15] had investigated TIG lap joining of 5A02 aluminum alloy to 304 stainless steel sheet with Zn–15%Al flux-cored filler wire. The results showed that fine Zn-rich phases uniformly distributed in the weld could enhance the joint strength, while coarse Zn-rich phases along the interfacial layer would degrade the bonding

* Corresponding author at: State Key Laboratory of Development and Application Technology of Automotive Steels, 201900 Shanghai, China.
*E-mail address:* jhuang@sjtu.edu.cn (J. Huang).

http://dx.doi.org/10.1016/j.matdes.2015.10.154
0264-1275/

strength of the interfacial layer. Zhang et al. [16] joined aluminum alloy to stainless steel by MIG welding-brazing method with 4047 AlSi12 filler metal, and showed that the thickness of IMC layer varied from 5 μm to 15 μm depending on the heat input. Yang et al. [17] had joined Al to zinc coated steel by cold metal transfer (CMT) method, and the results indicated that the IMC layer thickness in the CMT welds was well controlled below the 10 μm, which faciliated the achievement of relatively high weld strength. In addition, a pre-setting gap and an appropriate post-weld heat treatment could improve the weld strength. Reisgen et al. [18] showed that the low-alloy steel DC05 and the Al–3Mg alloy joint using electron beam welding method without filler metal could reach a maximum tensile strength of 200 MPa with a total IMC thickness of 2.3 μm. Considering the advantages such as high speed, precise control of low heat input offered by laser beam, laser brazing-fusion technology was investigated consequently. Dharmendra et al. [19] studied the effects of welding parameters on IMC layer. Shabadi et al. [20] joined an AA6061 aluminum sheet to a low-carbon galvanized steel sheet using laser pseudo-brazing method, and a zinc-based aluminum alloy was used as a filler wire. Joints produced using Al–Zn filler wire had a moderate strength, fractured at the heat affected zone of aluminum base metal, and had a thinner layer containing principally $Fe_2Al_5Zn_x$ type IMC of 10 μm. All the studies mentioned above concentrated on the relationship between the mechanical strength of Al/steel joint and the thickness of IMC layer. However, the mechanical strength of Al/steel welding-brazing joint cannot be simply correlated to the IMC layer thickness but also depends on the morphologies of IMC and the bonding area of brazing interface. Therefore, related contents would be studied in this work.

Butt joining of dissimilar metals of Al/steel have been investigated by us using fiber laser welding-brazing with ER4043 filler metal [21,22]. Different V-shaped bevel of 60° and 50° was fabricated on the mild steel, and a hot-dip galvanized process was performed to obtain a zinc coating at the steel's bevel surface before welding. The results indicated that it was feasible to join aluminum alloy to steel by butt joints. However, the tensile strength of the joint was low and average tensile strengths of 86.8 MPa (i.e., 60°) and 102.3 MPa (i.e., 50°) were obtained. In this study, butt joining of Al/steel with V-shaped bevel was conducted to improve the joint strength by using laser filler method. Different V-shaped bevel of 45° and 30° was fabricated on the mild steel, which was followed by an electro-galvanizing process of the steel to obtain a zinc coating at the steel's bevel surface before welding [23,24]. The objective of the present work is to evaluate the microstructure and mechanical strength of the Al/steel butt joint, and to achieve high joint strength by limiting the IMC layer and increasing the bonding area of Al/steel. After welding, firstly, the joining mechanism of the brazing interface was analyzed, and then the microstructures, especially the IMC structures at the interface with different bevel angle of the steel were characterized. Finally, the tensile strength of the joint was evaluated and fracture mechanisms of the joint were discussed.

## 2. Materials and experimental procedure

In this study, 2.5 mm thick AA6061 aluminum alloy and 2.5 mm thick Q235 low-carbon mild steel sheets with dimensions of 120 mm × 50 mm were used. Filler metal adapted was ER4043 welding wire (Al–5Si wt.%), with a diameter of 1.2 mm. The compositions of aluminum alloy, mild steel and filler wire are shown in Table 1. The groove of the joint was in the pattern "V"; a bevel angle of 60° was fabricated on the aluminum side and different bevel angles of 45° and 30° were fabricated on the mild steel side. The steel was coated with a pure zinc coating by electroplating before welding.

Laser welding was performed by a fiber laser with a peak power of 10 kW in the continuous mode (Model: YLS-10,000). The wire feeder was produced by Fronius (Trans Puls Synergic 5000). During welding process, the filler wire was fed in the leading edge of the molten, and the wire feed angle was adjusted to 30° to the sheet plane. The laser beam was tilted 12° ahead, i.e. in trailing position to reduce the risk of beam backscattering damage of the fiber, and the laser focus was adjusted to 20 mm above the surface of the workpiece (defocused condition), which resulted in a laser spot diameter of approximate 1.5 mm on the surface of the welding joint. Shielding argon gas was adopted at double sides of workpiece to avoid oxidation of weld metal, and a flow rate of 20 L/min and 5 L/min was used to protect the surface and bottom of the molten zone respectively. The setup of welding process was presented in Fig. 1. As shown, the filler wire and Al base metal were melted by the laser beam, and joining of the molten metal and solid steel was achieved in a butt joint configuration. Prior to welding, the steel sheets were degreased by acetone to remove grease or oil. Aluminum alloy sheets were brushed with a stainless steel brush to remove the oxide films on the surface first and then were degreased by acetone too. The welding speed (1.0 m/min) and laser power (5.0 kW) kept constant during welding process; three wire feeding speeds of 9.5 m/min, 9.8 m/min and 10.0 m/min were used respectively; bevel angles of 45° (Joint I) and 30°(Joint II) fabricated on the mild steel side were adopted.

To analyze the quality of Al/steel joint by laser welding-brazing process, the cross-sections of the specimens were prepared and examined. The polished Al/steel joint was etched by Dix–Keller solution. The microstructures of the weld were observed by scanning electron microscope (SEM, JSM-7600F) equipped with an energy-dispersive X-ray spectrometer (EDS).

Finally, tensile test specimens as shown in Fig. 2 were machined from a weldment and subjected to quasi-static testing in a Zwick T1-FR020TN-A50 mechanical tester. Load versus displacement curves were recorded as specimens were loaded at a stroke rate of 1 mm/min, and the joint strength was evaluated by the peak load. Three replicates were performed, and the average peak loads were reported. The fractured surfaces of the specimens after tensile testing were examined by SEM and EDS, and the phase present on the cracking interface was confirmed by a Cu X-ray radiation source (i.e., D8 ADVANCE) with a scattering angle ranging from 20 to 80° and a scan speed of 8°/min.

## 3. Results and discussion

### 3.1. Mechanism of the brazing interface of Al/steel butt joint

Laser joining Al to steel was performed using Al–Si filler metal. During the welding process, the laser spot was fixed on the tip of the filler metal as well as on the root of the bevel surface of Al sheet. Under laser beam heating, the zinc layer, which had been produced on the bevel surface of the steel by an electro-galvanizing process, was molten first and formed a thin liquid film. Then the filler metal was fed to the root of the bevel surface of Al sheet and touched upon the bevel surface.

**Table 1**
Nominal chemical compositions of AA6061 sheet, mild steel sheet and filler wire ER4043.

| Alloys | Elements/wt.% | | | | | | | | | | | |
|---|---|---|---|---|---|---|---|---|---|---|---|---|
| | Al | Ti | Mg | Si | Cu | Mn | Fe | Zn | Cr | C | P | S |
| AA6061 | Bal. | 0.15 | 0.8–1.2 | 0.4–0.8 | 0.15–0.4 | 0.15 | 0.7 | 0.25 | 0.04–0.35 | – | – | – |
| Mild steel | – | – | – | 0.5 | – | 2.5 | Bal. | – | – | 0.21 | 0.035 | 0.035 |
| ER4043 | Bal. | 0.2 | 0.05 | 4.5–6.0 | 0.3 | 0.05 | 0.8 | 0.1 | – | – | – | – |

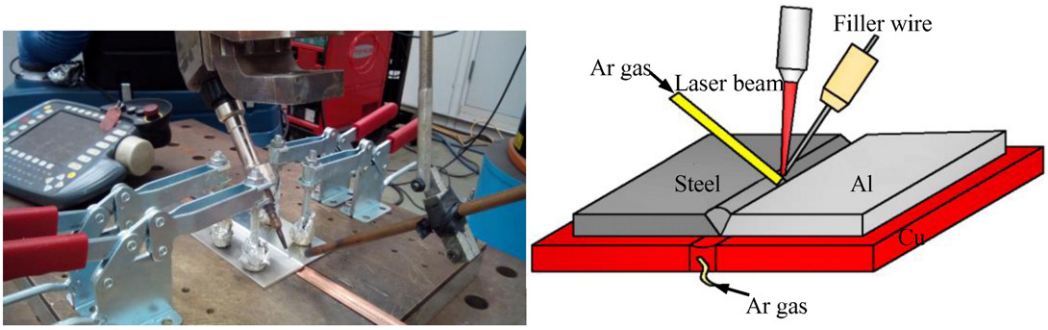


**Fig. 1.** Setup for laser welding of aluminum and steel.

When the filler metal was molten, it began to wet and spread on the steel surface due to the wetting action of liquid zinc film. The liquid filler metal spread from the root to the top of the bevel surface to form the seam.

Fig. 3 shows the schematic figure of cross-section of the typical Al/steel butt joint. As shown, the aluminum alloy sheet with low melting point was molten during the welding process, and it mixed with the molten filler metal to form the weld metal. The liquid weld metal spread on the steel sheet to form the brazing interface. As the brazing interface is significant to the mechanical performance of the joint [13], it will be analyzed in details. First, the mechanism of the brazing interface of Al/steel butt joints is analyzed. Then, the effect of the bevel angle of the steel on the microstructure of the brazing interface is presented.

The Zn coating had been driven from the steel surface towards the regions at the weld toe and root of the joint, thus zinc-rich regions were observed, as corresponding regions shown in Fig. 3. Microstructure of zinc-rich region is shown in Fig. 4(a). EDS analysis of this region has been conducted and the results are presented in Table 2. As shown, this region was mainly composed of Al matrix (location 1) and Al–Zn eutectoid (location 2) at the boundaries of α-Al solid solution. Many reports have shown that zinc coating can serve as a good interlayer former to achieve a sound Al/steel joint. Zinc-rich regions were also observed in other joints produced by several welding methods [1,5,24,25]. M. Gatzen et al. [26] thought that fluid-dynamic effects governed the accumulation of zinc towards the toe and root of the brazed metal. L. Agudo et al. [5] believed that Zn reactions on the steel sheet were oppressed under the presence of Al, Zn tended to escape, followed a capillary effect, and finally went through the cavity between the steel plate and the filler metal. Once the zinc contacted with the cold atmosphere, it rapidly solidified, resulting in the formation of zinc-rich region. The zinc layer was expected to be the key to the good wettability since it enabled the propagation of the aluminum on an almost liquid interface. It has been thought the zinc layer has some effects comparable to commercial fluxes to a certain degree. Firstly it can decrease the surface tension of the liquid. Secondly, the zinc layer can generate in situ a clean and oxide free metallic surface, which is important to inhibit the formation of new oxide layers on the aluminum melt during spreading process [27].

Apart from zinc rich regions at the weld toe and root, the brazing interface was mainly composed of Fe–Al IMC layer, as shown in Fig. 4(b). The Fe–Al phases at the brazing interface of Al/steel joint, which was obtained by different welding-brazing methods, have been studied. Lin et al. [10] revealed that the interface was made up of two kinds of Fe–Al IMCs. Further investigations by L. Agudo et al. [5] and H. Springer et al. [28] showed that the orthorhombic $Fe_2Al_5$ (η-phase) which possessed the pronounced columnar characteristic, grew orthogonally to the joint area into the steel. In addition, the monoclinic crystal of the $FeAl_3$ (θ-phase) were formed adjacent to the weld metal. In the present experiment, two kinds of IMC layers with different contrast were seen in Fig. 4(b), as the layers i and ii shown in Fig. 4(b). EDS linear scanning analysis along the line ab was carried out to analyze the compositions of the sub-layers and the results were also shown in Fig. 4(b). In generally, it was found that the distribution ratio of Fe/Al kept unchanged in the reaction layer i. In the layer ii, the distribution ratio of Fe/Al kept unchanged at first, but the Fe content decreased whereas the Al content increased when reaching the transition zone between the layer ii and weld metal. EDS analysis was performed at locations 3 and 4 of the brazing interface, and the results verified that these two sub-layers corresponded to $Fe_2Al_5$ in the layer i and $FeAl_3$ in the layer ii. In addition, the $Fe_2Al_5$ and $FeAl_3$ sub-layers showed different contrast in SEM observation in Fig. 4(b). Su et al. [29] explained that because of the microhardness difference between $FeAl_3$ (700 HV) and $Fe_2Al_5$ (1100 HV), terrace would generate between $FeAl_3$ and $Fe_2Al_5$ after polishing process, resulting in different contrast in SEM observation. There have been several studies to analyze the formation of Fe–Al IMC at the brazing interface [30,31]. The results revealed that $Fe_2Al_5$ phase was identified to be formed in the first place, and its growth was found to be mainly controlled by a diffusion regime between Al and Fe; while $FeAl_3$ was formed subsequently, and it grew under a kinetic regime between Al and $Fe_2Al_5$. Besides, the parabolic and linear rate constants of $Fe_2Al_5$ and $FeAl_3$ were identified respectively. Moreover, in Fig. 4(b), Si element was found to be concentrated in the $Fe_2Al_5$, which could be seen from the occurrence of peak value of green line in the layer i. Dong et al. [23] and Song et al. [32] had studied the influence of alloy elements on microstructure and

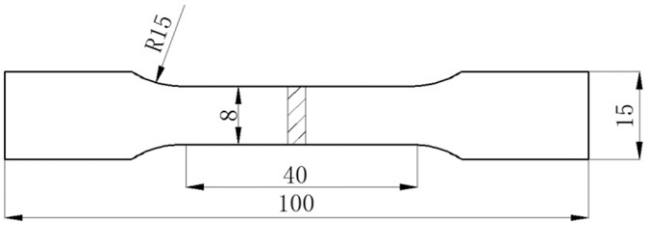


**Fig. 2.** Specimen machined from welded Al-steel sheet (dimensions in mm).

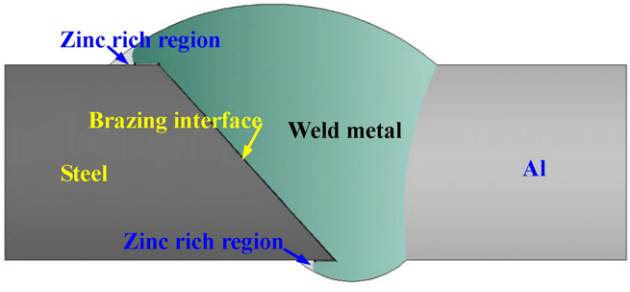


**Fig. 3.** Schematic of the cross-section of Al/steel butt joint.

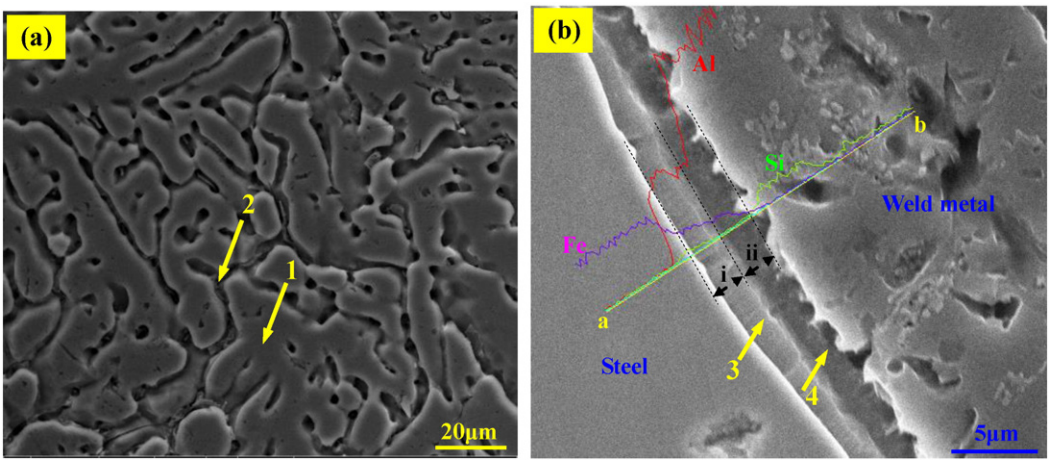


**Fig. 4.** Microstructure of the brazing interface: (a) zinc-rich region; (b) Fe–Al IMC layer.

mechanical property of Al/Steel joint. The results showed that the Si addition had a great effect in preventing the building-up of the IMC layer, and minimizing its thickness. According to investigations by Yin et al. [33], crystalline $Fe_2Al_5$ orthorhombic structure contained 30% voids along the c-axis, and the diffusion of Si into the reactive layer and occupation of the vacancies of the $Fe_2Al_5$ phase could greatly reduce the Al diffusion capability and the Fe–Al reaction rate.

### *3.2. Microstructures of the brazing interface for Joints I and II*

During the welding process, the thermal cycles for different regions of the brazing interface were different because the laser welding-brazing was a local heating process [34]. It caused different reaction time and temperature for different regions at the interface, which resulted in the interfacial reaction nonhomogeneity of the joint. A. Szczepaniak [35] showed that the peak temperature had significantly stronger influence on the thickness of the IMC reaction layer than cooling time. As the property of joint depended on the type of IMC, the morphology and thickness [31], it was necessary to observe and analyze the brazing interface of different positions for individual joint. The wire feeding speed had smaller effect on the microstructures when laser power of 5.0 kW was used, thus two typical joints obtained at a wire feed rate of 10 m/min were chosen to compare the microstructures of Joints I and II. Figs. 5 and 6 present the microstructures of different regions for these two joints. The characteristic of each region will be discussed in detail.

Fig. 5 shows the microstructures of different regions for Joint I. Among them, Fig. 5 (a) shows the cross-section of the typical joint, and Fig. 5 (b)–(h) show the enlarged images corresponding to different regions demonstrated in Fig. 5(a). At the top region A shown in Fig. 5(b), the long distance from the laser heating spot brought relatively low temperature and short reaction time between steel and weld metal, which caused thin IMC layer (~4 μm) in this region. At the region B shown in Fig. 5(c) and (d), heterogeneous layer was formed. It was observed that the interface between the steel substrate and the $Fe_2Al_5$ layer was smooth, while the boundary between $FeAl_3$ and the weld metal was made of irregularities orientated towards the weld metal. In addition, seen from Fig. 5(c), thin needles and platelets of $FeAl_3$ were found to be dispersed near the interface. The platelets attached to the outer part of the $FeAl_3$ layer and grew in columnar shape into the molten weld metal. K. Bouche et al. [36] thought that thin needles and platelets of $FeAl_3$ were formed by eutectic reaction during the solidification of the melt, because the melt contained some amount of dissolved Fe. However, H. R. Shahverdi et al. [30] held a different opinion. They thought the $FeAl_3$ layer would break and enter into the weld metal. The breakage of IMCs and subsequent floating of these blocks within molten weld metal provided the iron required for the formation of intermetallic needles near the interface. Moreover, several cracks were observed in the $Fe_2Al_5$ layer; their crack initiation seemed to take place between the individual columns of the $Fe_2Al_5$ phase and from there the cracks propagated across the entire $Fe_2Al_5$ sub-layer. The crack might be caused by the longitudinal elongation coefficient which was, compared with steel, twice as high. The shrinkage which occurred with varying speed during cooling caused strong stresses, combined with the almost non-existent ductility of IMCs, led to cracks produced. Bozzi et al. [37] also found that micro-cracks were generated when IMC layer was around 8 μm, but they could not induce fracture of the joint. The IMC thickness in this region varied from 8 μm to 10 μm. In addition, it was found that the thickness of $Fe_2Al_5$ sub-layer was significantly larger than that of the $FeAl_3$ sub-layer, but they kept in the same order of magnitude here. However, in the IMC layers on hot-dipped steel and in diffusion couples, the thickness of $Fe_2Al_5$ sub-layer exceeded that of $FeAl_3$ sub-layer by up to several orders of magnitude [36].

Fig. 5 (e)presents the microstructures of region C. Because the steel matrix was slightly molten here, strong interfacial reaction between liquid weld metal and steel occurred, thus IMC layer with a maximum thickness of 25 μm was formed. It was found that the $Fe_2Al_5$ sub-layer occupied most part of IMC layer, while only a thin $FeAl_3$ sub-layer (less than 3 μm) was produced. An obvious crack which was parallel to the brazing interface was formed and propagated through the entire layer. Fig. 5 (f) shows the microstructure in the middle part of the interfacial layer (region D) of the joint. The thickness of the layer in this region was about 4 μm in average. The thickness of $FeAl_3$ sub-layer became thicker (~2 μm), which was almost the same width with that of $Fe_2Al_5$ sub-layer.

Fig. 5 (g) and (h) present the microstructures at the bottom of the joint, as region E shown in Fig. 5(a). The region E was mainly composed of $Fe_2Al_5$, with very thin $FeAl_3$ layer formed. Observed from Fig. 5(g), large amount of white granular phase was formed between $Fe_2Al_5$ layer and steel substrate, and EDS analysis showed the possible phase

**Table 2**
EDS results of zones 1–4 in Fig. 4.

| Location | Al (at.%) | Si (at.%) | Fe (at.%) | Zn (at.%) | Possible phase |
|---|---|---|---|---|---|
| 1 | 97.94 | 1.21 | 0 | 0.84 | α-Al solid solution |
| 2 | 89.08 | 0.64 | 0 | 10.28 | Al–Zn eutectoid |
| 3 | 68.20 | 5.77 | 25.04 | 0 | $Fe_2Al_5$ |
| 4 | 77.52 | 0.92 | 21.56 | 0 | $FeAl_3$ |

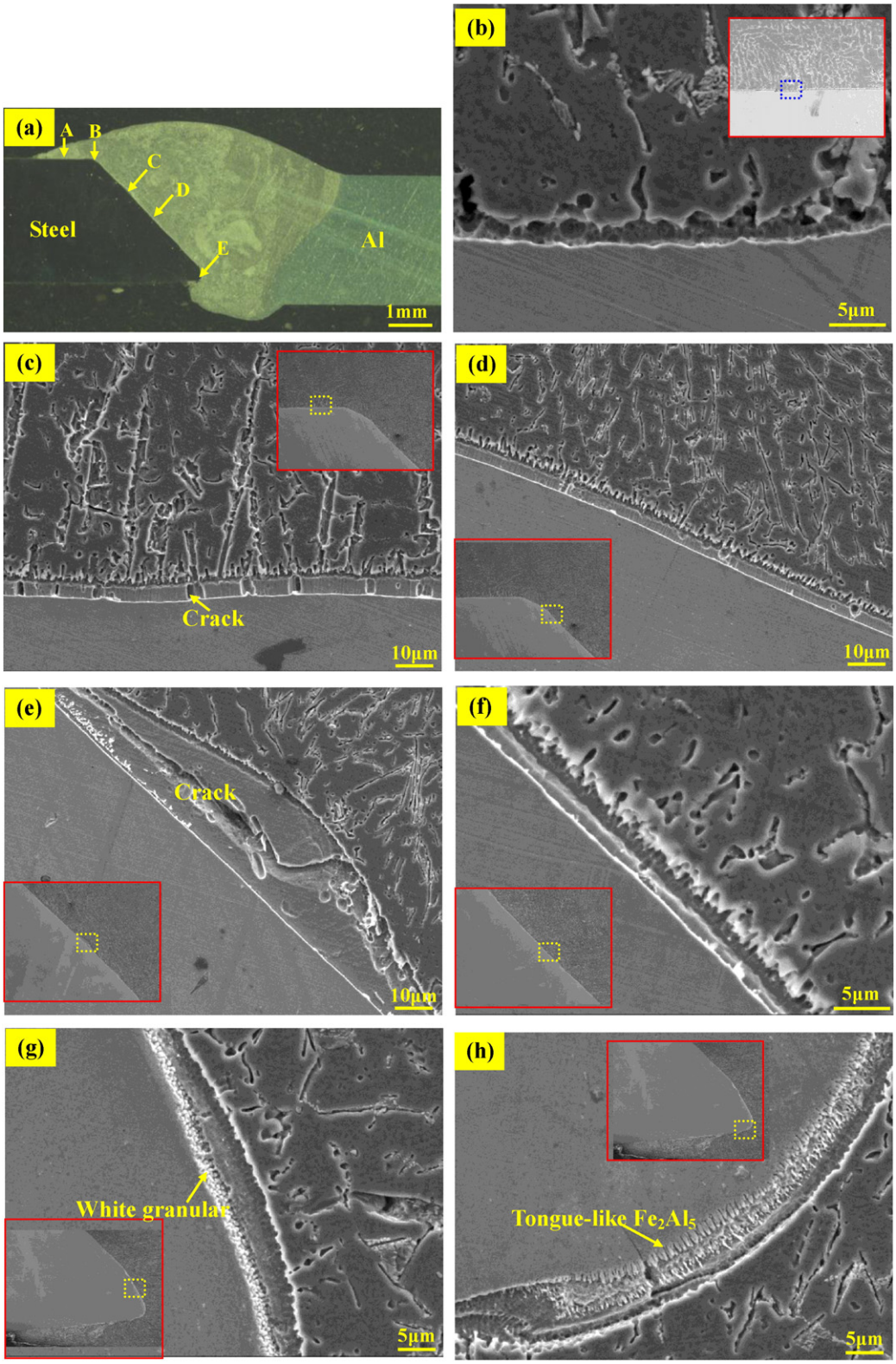


**Fig. 5.** Microstructure of the brazing interface for Joint I: (a) cross-section, (b) zone A, (c) and (d) zone B, (e) zone C, (f) zone D, (g) and (h) zone E.

was Si-rich Fe–Al IMC. The formation mechanism of this phase needs to be further analyzed. The morphology of the IMC in region E was obviously different from other regions. The interface morphology of $Fe_2Al_5$/weld metal in Fig. 5(h) became irregular, and a tongue-like interface with peaks orientated towards steel was formed. Similar phenomenon had been observed by other researchers [5,35,38,39], and the tongue-like interface seemed to be concerned with the formation process of $Fe_2Al_5$ as well as the surrounding temperature. Heumann and Dittrich [38] explained that this tongue-like interface was a result of favorable possibilities for aluminum atoms to diffuse along the c-axis direction of $Fe_2Al_5$ orthorhombic structure on structural vacancies. L. Agudo et al. [5] thought that not the orientation of the longest axis

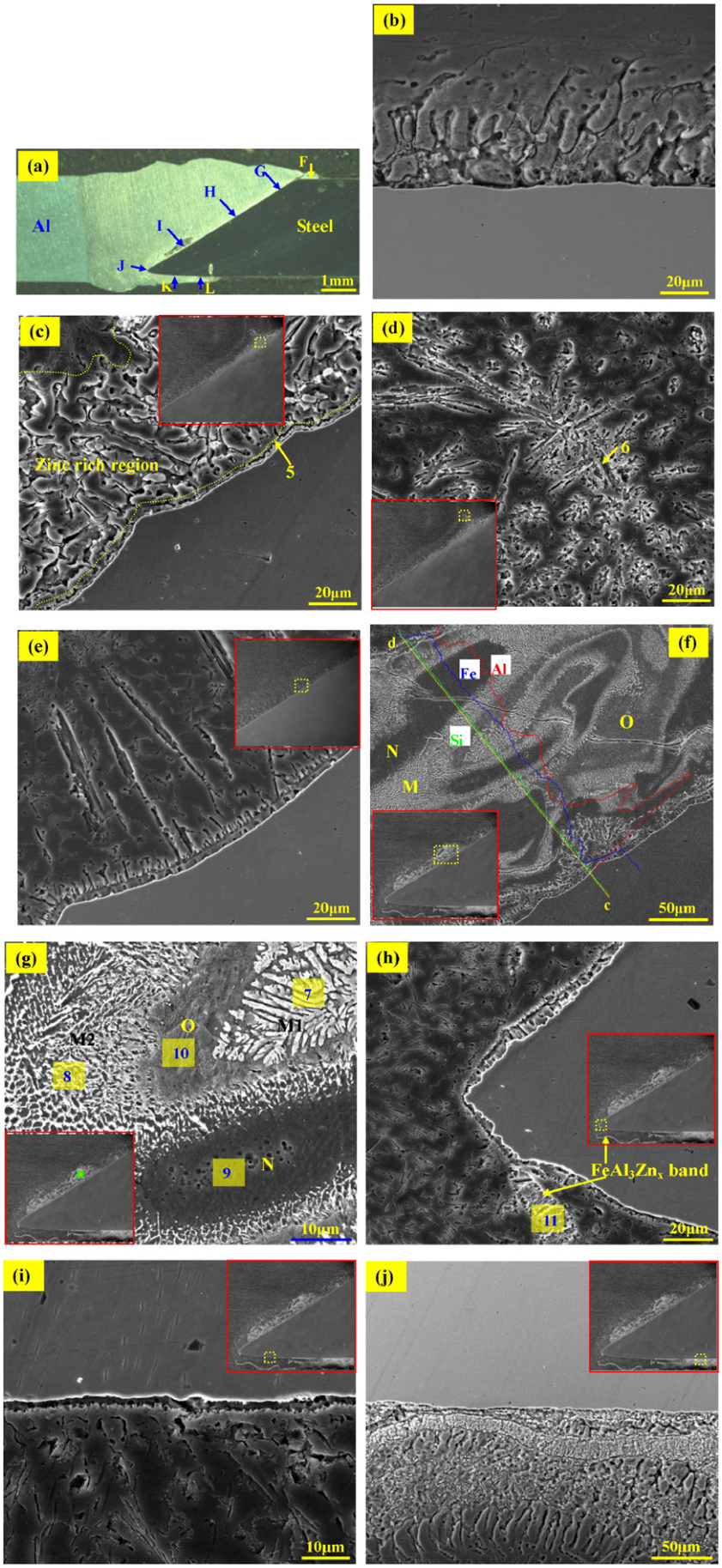


**Fig. 6.** Microstructure of the brazing interface for Joint II: (a) cross-section, (b) zone F, (c) and (d) zone G, (e) zone H, (f) and (g) zone I, (h) zone J, (i) zone K and (j) zone L.

**Table 3**
EDS results of zones 5–11 in Fig. 6.

| Location | Al (at.%) | Si (at.%) | Zn (at.%) | Fe (at.%) | Possible phase |
|---|---|---|---|---|---|
| 5 | 70.37 | 4.23 | 3.17 | 22.03 | $Fe_2Al_5Zn_x$ |
| 6 | 77.32 | 4.63 | 0 | 18.05 | $FeAl_3$ |
| 7 | 55.66 | 3.37 | 0 | 40.97 | $Fe_2Al_5 + FeAl_3$ |
| 8 | 62.31 | 8.29 | 0 | 29.4 | $FeAl_3 + Al_8Fe_2Si$ |
| 9 | 75.94 | 1.08 | 0 | 22.97 | $FeAl_3$ |
| 10 | 60.77 | 2.05 | 0 | 37.18 | $\alpha$-Al + $FeAl_3 + Al_8Fe_2Si$ |
| 11 | 76.61 | 0 | 7.38 | 16.01 | $FeAl_3Zn_x$ |

of $Fe_2Al_5$ but rather the preferential nucleation conditions induced the serrated structure of the steel-$Fe_2Al_5$ interface. In addition, Eggeler et al. [39] showed that this face irregularity would gradually conform to a planar shape when the temperature of aluminum melt increased. A. Szczepaniak [35] also found that increase in the amount of applied heat changed the morphology of the Fe–Al IMC layer and the interface tends to flatten with increasing heat input. The IMC thickness in region E varied from 5 μm to 10 μm along the interface.

Therefore, when a bevel angle of 45° of the steel was used, the morphology and thickness of the layer was not constant but varied along the interface. The thickness of most part of the brazing interface was controlled to be less than critical value of 10 μm in Ref. [2]. Except for the bottom, the interface between $FeAl_3$ and weld metal kept irregular while the interface between $Fe_2Al_5$ and steel kept almost flat.

After the brazing interface of Joint I was observed, the interface of Joint II was also examined for comparison. Fig. 6 (a) shows the cross-section of the joint, and Fig. 6(b)–(j) show the enlarged images corresponding to different regions demonstrated in Fig. 6(a). Fig. 6 (b) presents the upper region F of the joint. EDS analysis showed zinc rich zone was formed here, and typical Al–Zn eutectoid was observed. However, no Fe–Al IMCs was formed in this region. Fig. 6 (c) and (d) show the region G on the bevel face. Fig. 6 (c) reveals that a thin brazing interface of 4 μm was formed. According to EDS result of location 5, the possible phase was $Fe_2Al_5Zn_x$. In addition, the zinc-rich zone with a maximum content of 15.62 at. Pct. Zn was also formed in the weld metal near the brazing interface. However, in the weld metal adjacent to the zinc rich region, many platelets of $FeAl_3$ (location 6) were formed, as shown in Fig. 6(d). Seen from the brazing interface in Fig. 6(c), the steel was slightly molten during the welding process, thus the Fe atom entered into the weld metal and formed $FeAl_3$ after solidification. Compared to Fe, Al had a larger affinity to Zn [40], which could explain why Al–Zn eutectoid phases were formed near the brazing interface.

Fig. 6 (e) shows the brazing interface in the middle part of the bevel face. As shown, the layer here was composed of $Fe_2Al_5$ and $FeAl_3$ sublayers with an entire thickness of 7 μm in average; some platelets of $FeAl_3$ crystals were also produced near the interface. Fig. 6 (f) and (g) show the microstructures of region I. As direct laser radiation occurred in this region, a large amount of Fe–Al IMC was formed, which reached about 1 mm parallel to the interface and a maximum thickness of 265 μm perpendicular to the interface. Observed from Fig. 6(f), this region was mainly consisted of the white area M, the dark area N and the gray area O. EDS linear scanning analysis along the line c–d was conducted and the results were also shown in Fig. 6(f). According to the result, this region was mainly composed of Fe, Al and Si elements; the distribution ratio of Fe/Al in the dark area was smaller than that in the white area; the distribution ratio of Fe/Al in the gray area was in the transition zone between them. In addition, the Si content increased slightly in the white area compared that in the dark area. Due to thicker Fe–Al IMC layer formed and higher stress generated here during cooling process, an obvious crack was produced, which traversed across the entire brittle layer. Fig. 6(g) presents enlarged image of this region. EDS analysis was also conducted to understand the possible phases formed in each region, and the results were listed in Table 3. As shown, the white area was mainly composed of two parts (i. e., M1 and M2). Among them, the dendrite crystals were formed in the region M1, which grew towards the gray area. The result of EDS analysis of location 7 showed region M1 was mainly composed of $Fe_2Al_5$ and $FeAl_3$. However, the morphology in the white region M2 was different from M1, which consisted of band-shaped or net-shaped white phase and the dark phase between them. Based on EDS result of location 8 in the region M2, $FeAl_3$ and $Al_8Fe_2Si$ phases were produced. The dark region N was mainly composed of $FeAl_3$, while the gray region O was mainly composed of α-Al, $FeAl_3$ and $Al_8Fe_2Si$. Thus, various Fe–Al phases with different morphologies were formed.

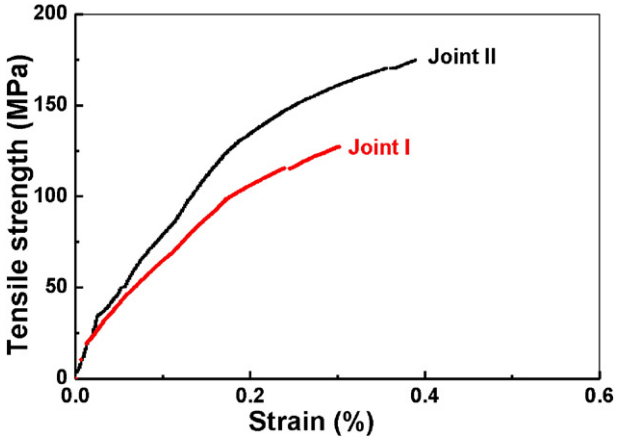


**Fig. 8.** Stress–strain curves obtained for Al/steel butt joints.

Fig. 6 (h) presents the microstructures at the bottom of the joint. Both $Fe_2Al_5$ and $FeAl_3$ were produced here. The thickness of $FeAl_3$ sublayer was very thin. The interface between $Fe_2Al_5$ and steel also became serrated, but it was less irregularity compared with that in Fig. 5(h). The layer was non-homogeneous, with a maximum thickness of 8 μm. In addition, a long bright band was formed at the bottom of the steel seen from Fig. 6(h), which has a width of about 10 μm, and no crack was found in the band; the result of EDS analysis in location 11 showed $FeAl_3Zn_x$ was formed. The $FeAl_3Zn_x$ was not so compact, and there existed some α-Al in it.

Furthermore, except for zinc rich region (i.e., Fig. 6(j)) formed at the lower platform of the joint, a brazing interface with a thickness of 3 μm was also formed, as shown in Fig. 6(i). Thus, complex Fe–Al IMCs with heterogeneous morphologies were formed at the brazing interface for Joint II. Although thicker IMC layer formed in region I, the thickness was well controlled to be less than 10 μm in other regions.

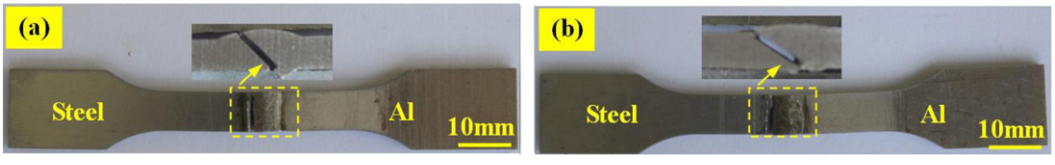


**Fig. 7.** Fracture location for the joint with a bevel angle of: (a) 45° and (b) 30°.

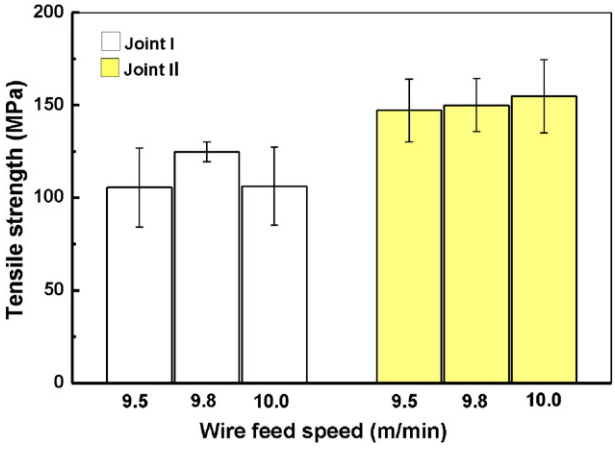


**Fig. 9.** Tensile strength of the specimens with constant laser power of 5 kW.

The relationship between the IMC layer and the tensile strength of the Al/steel joint has been studied by Borrisutthekul et al. [41], and it was found that the joint strength increased with decreasing thickness of the reaction layer. In this study, the average IMC thickness was 5.50 μm for Joint I and 8.29 μm for Joint II. In addition, a relatively large region composed of Fe–Al IMCs was formed near the interface for Joint II. These might be detrimental to the tensile strength for the Joint II. However, according to the dimension of the tensile specimen shown in Fig. 2, the bonding area for Joint I was 28.28 $mm^2$, and the bonding area for Joint II was 40 $mm^2$. Thus the Joint II has a larger bonding area than that of the Joint I, which could contribute to a higher tensile strength of this joint on the other hand. Which factor has a bigger influence on the tensile strength of the steel/Al joint? This will be evaluated by the tensile test.

### 3.3. Tensile strength of laser butt joint of aluminum and steel

Tensile tests were carried out in order to compare the tensile strength of the joints. All the joints failed at the brazing interface, as shown in Fig. 7. During the tensile test, the crack firstly initiated at the weld root of the joint, and propagated along the bevel surface of Fe–Al IMC layer. Finally, it propagated to the weld metal at the upper platform of the joint, which led to the failure of the joint.

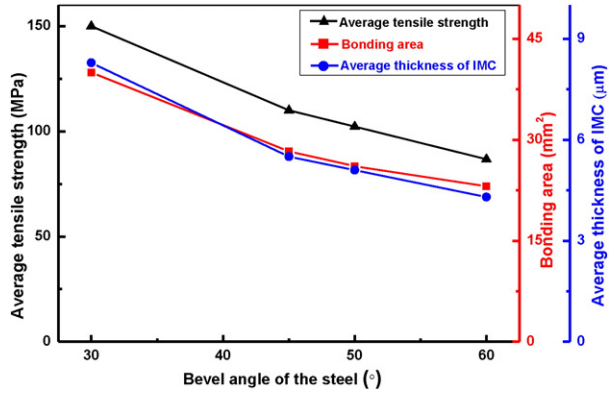


**Fig. 10.** The results of (a): different bevel angle of the steel (30°, 45°, 50° and 60°) vs. average tensile strength, bonding area and average thickness of IMC for Al/steel joints [21,22].

The maximum tensile strengths of 130 MPa and 174 MPa were obtained for these two joints, and Fig. 8 shows the corresponding stress–strain curves of Joints I and II. Even though the failure of all samples was always located at the brazing interface during the mechanical test, the specimen endured some plastic deformation. As shown in Fig. 8, the plastic deformation of the Joint II is larger than that of the Joint I.

To compare the effects of wire feed speed and bevel angle on the tensile strength, the results of tensile tests versus wire feed speed with constant laser power of 5 kW are shown in Fig. 9. It was obvious that the tensile strength for the joint with a bevel angle of 30° was higher than that with a bevel angle of 45°. The average tensile strengths of Joints I and II were 110 MPa and 150 MPa respectively.

As introduced in Refs. [21,22], butt joining of dissimilar metals of Al/steel have been conducted using fiber laser welding-brazing with ER4043 filler metal. Bevel angles of 60° and 50° of the steel were used. The bonding area was calculated and the average IMC thickness of the joint was measured, and the results of different bevel angle of the steel vs. average tensile strength, bonding area and average thickness of IMC were shown in Fig. 10. In addition, the results of this study were also included in Fig. 10 for comparison. It was found that the average tensile strength, the bonding area and the average thickness of IMC decreased with increasing bevel angle of the steel. It was known that the thickness of IMC and the bonding area have a great influence on the tensile strength of Al/steel joint [2,42]. Thus, the relationship between the average tensile strength, the bonding area and the average thickness of IMC would be analyzed.

As shown in Fig. 10, the average thickness of IMC changed from 8.29 μm to 4.3 μm when the bevel angle of the steel increased from 30° to 60°. Though thicker IMC layer (8.29 μm) was formed when the bevel angle of the steel was 30°, it was considered to be within an acceptable range because Kobayashi et al. [43] have shown that the critical thickness of the Fe–Al layer was 10 μm. In addition, with increasing bevel angle of the steel from 30° to 60°, the bonding area of the joint decreased from 40 $mm^2$ to 23.1 $mm^2$, and the average tensile strength decreased from 150 MPa to 86.8 MPa. Thus, the tensile strength increased with increasing bonding area of Al/steel joint.

Fig. 11 shows typical results from SEM investigations of fracture surfaces of the interfacial failure in the Al/steel butt joint. Chemical compositions of location 12–15 obtained from EDS measurements are listed in Table 4. Fig. 11(a) presents the fracture surface at the upper side of the joint. As shown, three types of fractures can be differentiated. The first one was the weld metal region (location 12). As this region was the final failure location of the joint during tensile test, clear torn lines on the fracture surface were observed. The second region presents the typical cleavage fracture mode with river pattern strips of particular orientation on the fracture surface. The region between the first region and second region was the transitional region, where both the weld metal and the Fe–Al layer could be found. Fig. 11(b) shows the fracture surface of weld metal at the transitional region. According to the results of EDS analysis, this region was composed of α-Al solid solution (location 13) and Al–Si grain boundaries (location 14). Fig. 11(c) also shows the cleavage fracture mode on the bevel surface, which occupied the largest fraction area of the sample surface exhibiting interfacial failure. The chemical composition of 72.14 at. Pct. Al, 24.32 at. Pct. Fe and 3.55 at. Pct. Si was analyzed on the cleavage surface, matching the composition of $Fe_2Al_5$. To further confirm the phase, XRD analysis at the cracking interface was performed and the result is shown in Fig. 11(d). As revealed, $Fe_2Al_5$ was found on the crack surface. Thus the crack might initiate and propagate in the $Fe_2Al_5$ layer during the tensile process. Similarly, H. Springer et al. [6] observed the crack propagated in the brittle IMCs and cut through remains of steel at the irregular, wavy steel/η interface of Al/steel joint. The same result was also found by Song et al. [13]. However, he thought the crack derived from the top part of brittle $Fe_2Al_5$ interfacial layer, which was different from the result in this study.

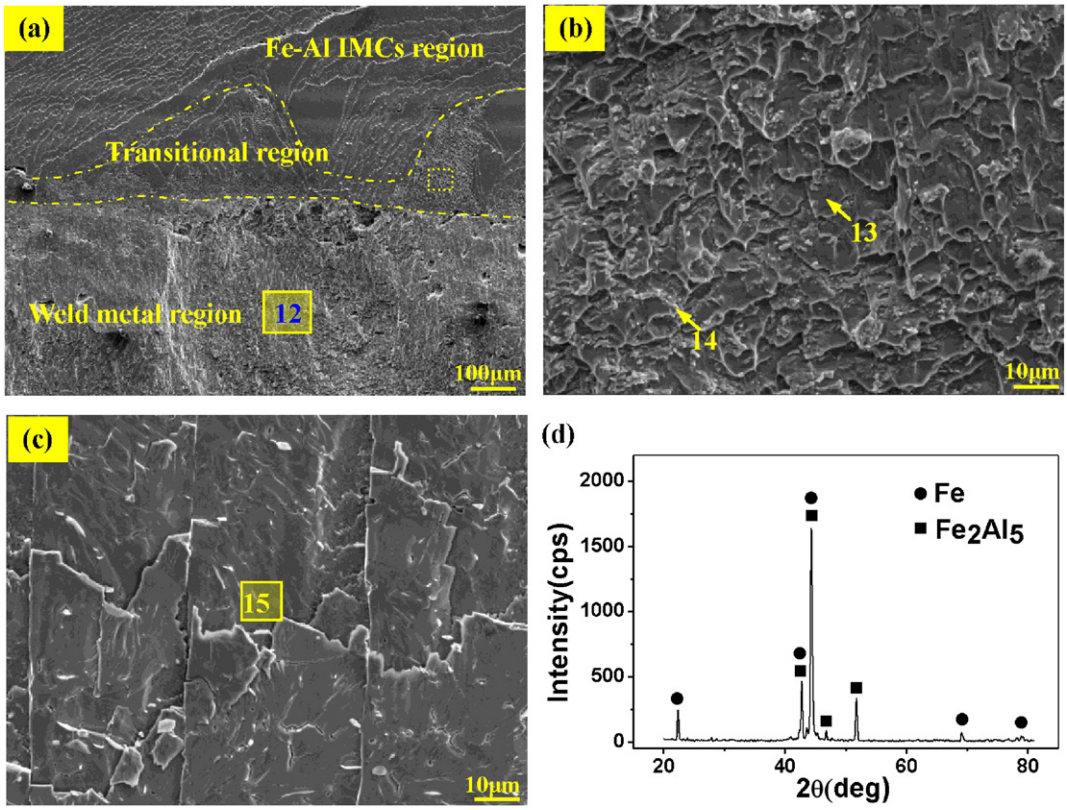


**Fig. 11.** Fractography of the Joint II: (a) upper side; (b) enlarged transitional region in Fig. 11 (a); (c) bevel surface and (d) XRD analysis of the cracking interface.

## 4. Conclusions

According to the analysis of the brazing interface and tensile strength of Al/steel butt joint with different bevel angles of the steel, conclusions can be drawn as follows:

(1) A butt joint of Al/steel was obtained using laser welding-brazing method. Zinc rich regions were produced at the toe and root of the joint. The zinc layer enabled the propagation of the aluminum on an almost liquid interface. The brazing interface was mainly composed Fe–Al IMC, with the formation of η-$Fe_2Al_5$ phase close to the steel and θ-$FeAl_3$ phase adjacent to the weld metal, and the $Fe_2Al_5$ sub-layer was much thicker as compared to $FeAl_3$. Si element was concentrated in the $Fe_2Al_5$ sublayer.

(2) The thickness and morphology of the IMC reaction layer was not constant but varied along the brazing interface. When a bevel angle of 45° was adopted, the interface between the steel substrate and the $Fe_2Al_5$ layer was smooth, while the boundary between $FeAl_3$ and the weld metal was made of irregularities orientated towards the weld metal for the upper and middle interface; thin needles and platelets of $FeAl_3$ were also found to be dispersed in some regions near the interface; a tongue-like interface with peaks orientated towards steel was formed between $Fe_2Al_5$ and steel for the lower interface; the IMC thickness of most part of the brazing interface was controlled to be less than 10 μm.

(3) The morphology of the IMC reaction layer of joint with a bevel angle of 30° was more complex than that of joint with a bevel angle of 45°, and the average IMC thickness was 5.50 μm for the joint with a bevel angle of 45° and 8.29 μm for the joint with a bevel angle of 30°. The bonding area for the joint with a bevel angle of 45° was 28.28 $mm^2$, and the bonding area for the joint with a bevel angle of 30° was 40 $mm^2$.

(4) All the joints failed in the $Fe_2Al_5$ layer of the brazing interface, which presented typical cleavage fracture mode. The mechanical strength of Al/steel welding-brazing joint cannot be simply correlated to the IMC layer thickness but also depended on the bonding area. The average tensile strengths of joint with a bevel angle of 30° and joint with a bevel angle of 45° were 150 MPa and 110 MPa respectively.

**Table 4**
EDS results of zones 12–15 in Fig. 11.

| Location | Al (at.%) | Si (at.%) | Zn (at.%) | Fe (at.%) | Possible phase |
|---|---|---|---|---|---|
| 12 | 90.34 | 7.32 | 2.34 | 0 | – |
| 13 | 98.75 | 1.25 | 0 | 0 | α-Al solid solution |
| 14 | 95.55 | 3.67 | 0.77 | 0 | Al–Si eutectic |
| 15 | 72.14 | 3.55 | 0 | 24.32 | $Fe_2Al_5$ |

## Acknowledgments

The authors would like to thank the financial support of the State Key Laboratory of Development and Application Technology of Automotive Steels (13R003ECEQ), without which this work would have been impossible.

## References

[1] Y.C. Su, X.M. Hua, Y.X. Wu, Effect of input current modes on intermetallic layer and mechanical property of aluminum-steel lap joint obtained by gas metal arc welding, Mater. Sci. Eng. A 578 (2013) 340–345.
[2] R. Cao, Q. Huang, J.H. Chen, P.C. Wang, Cold metal transfer spot plug welding of AA6061-T6-to-galvanized steel for automotive applications, J. Alloys Compd. 585 (2014) 622–632.

[3] A. Szczepaniak, J.F. Fan, A. Kostka, D. Raabe, On the correlation between thermal cycle and formation of intermetallic phases at the interface of laser-welded aluminum-steel overlap joints, Adv. Eng. Mater. 14 (2012) 464–472.
[4] S. Meco, G. Pardal, S. Ganguly, S. Williams, N. Mcpherson, Application of laser in seam welding of dissimilar steel to aluminum joints for thick structural components, Opt. Lasers Eng. 67 (2015) 22–30.
[5] L. Agudo, D. Eyidi, C.H. Schmaranzer, E. Arenholz, Intermetallic $Fe_xAl_y$-phases in a steel/Al-alloy fusion weld, J. Mater. Sci. 42 (2007) 4205–4214.
[6] H. Springer, A. Kostka, J.F. dos Santos, D. Raabe, Influence of intermetallic phases and Kirkendall-porosity on the mechanical properties of joints between steel and aluminum alloys, Mater. Sci. Eng. A 5 (2011) 4630–4642.
[7] Y.F. Sun, H. Fujii, N. Takaki, Y. Okitsu, Microstructure and mechanical properties of dissimilar Al alloy/steel prepared by a flat spot friction stir welding technique, Mater. Des. 47 (2013) 350–357.
[8] X. Liu, S. Lan, J. Ni, Analysis of process parameters effects on friction stir welding of dissimilar aluminum alloy to advanced high strength steel, Mater. Des. 59 (2014) 50–62.
[9] P. Prangnell, F. Haddadi, Y.C. Chen, Ultrasonic spot welding of aluminum to steel for automotive application — microstructure and optimisation, Mater. Sci. Technol. 27 (2011) 617–624.
[10] Y. Abe, T. Kato, K. Mori, Self-piercing riveting of high tensile strength steel and aluminum alloy sheets using conventional rivet and die, J. Mater. Process. Technol. 209 (2009) 3914–3922.
[11] Y.C. Lim, L. Squires, T.Y. Pan, M. Miles, G.L. Song, Y. Wang, Z. Feng, Study of mechanical joint strength of aluminum alloy 7075-T6 and dual phase steel 980 welded by friction bit joining and weld-bonding under corrosion medium, Mater. Des. 69 (2015) 37–43.
[12] F. Findik, Recent developments in explosive welding, Mater. Des. 32 (2011) 64–72.
[13] J.L. Song, S.B. Lin, C.L. Yang, G.C. Ma, H. Liu, Spreading behavior and microstructure characteristics of dissimilar metals TIG welding-brazing of aluminum alloy to stainless steel, Mater. Sci. Eng. A 509 (2009) 31–40.
[14] H.G. Dong, C.Q. Liao, L.Q. Yang, C. Dong, Effects of post-weld heat treatment on dissimilar metal joint between aluminum alloy and stainless steel, Mater. Sci. Eng. A 550 (2012) 423–428.
[15] H.G. Dong, L.Q. Yang, C. Dong, S.D. Kou, Arc joining of aluminum alloy to stainless steel with flux-cored Zn-based filler metal, Mater. Sci. Eng. A 527 (2010) 7151–7154.
[16] H.T. Zhang, J.K. Liu, Microstructure characteristics and mechanical property of aluminum alloy/stainless steel lap joints fabricated by MIG welding-brazing process, Mater. Sci. Eng. A 528 (2011) 6179–6185.
[17] S.L. Yang, J. Zhang, J. Lian, Y.P. Lei, Welding of aluminum alloy to zinc coated steel by cold metal transfer, Mater. Des. 49 (2013) 602–612.
[18] U. Reisgen, C. Otten, J. Schonberger, Investigations about the influence of time-temperature curve on the formation of intermetallic phases during electron beam welding of steel-aluminum material combinations, Weld. World 58 (2014) 443–454.
[19] C. Dharmendra, K. Rao, J. Wilden, S. Reich, Study on laser welding-brazing of zinc coated steel to aluminum alloy with a zinc based filler, Mater. Sci. Eng. A 528 (2011) 1497–1503.
[20] R. Shabadi, M. Suery, A. Deschamps, Characterization of joints between aluminum and galvanized steel sheets, Metall. Mater. Trans. A 44 (2013) 2672–2682.
[21] J.H. Sun, Q. Yan, W. Gao, J. Huang, Investigation of laser welding on butt joints of Al/steel dissimilar materials, Mater. Des. 83 (2015) 120–128.
[22] W. Gao, Q. Yan, J. Huang, Microstructure and mechanical property of laser wire fusion brazing welded butt joints of steel-aluminum dissimilar metal, Chin. J. Lasers 41 (2014) 1–6.
[23] H. Dong, W. Hu, Y. Duan, X. Wang, C. Dong, Dissimilar metal joining of aluminum alloy to galvanized steel with Al–Si, Al–Cu, Al–Si–Cu and Zn–Al filler wires, J. Mater. Process. Technol. 212 (2012) 458–464.
[24] R. Cao, G. Yu, J.H. Chen, P.C. Wang, J. Mater. Process. Technol. 213 (2013) 1753–1763.
[25] G.L. Qin, Z. Lei, B.L. Su, X.M. Meng, S.Y. Lin, Large spot laser assisted GMA brazing-fusion welding of aluminum alloy to galvanized steel, J. Mater. Process. Technol. 214 (2014) 2684–2692.
[26] M. Gatzen, T. Radel, C. Thomy, F. Vollertsen, Wetting behavior of eutectic Al–Si droplets on zinc coated steel substrates, J. Mater. Process. Technol. 214 (2014) 123–131.
[27] M. Gatzen, T. Radel, C. Thomy, F. Vollertsen, The role of zinc layer during wetting of aluminum on zinc-coated steel in laser brazing and welding, Phys. Procedia 56 (2014) 730–739.
[28] H. Springer, A. Kostka, E.J. Payton, D. Raabe, A. Kaysser-Pyzalla, G. Eggeler, On the formation and growth of intermetallic phases during interdiffusion between low-carbon steel and aluminum alloys, Acta Mater. 59 (2010) 1586–1600.
[29] Y.C. Su, X.M. Hua, Y.X. Wu, Influence of alloy on microstructure and mechanical property of aluminum-steel lap joint made by gas metal arc welding, J. Mater. Process. Technol. 214 (2014) 750–755.
[30] H.R. Shahverdi, M.R. Ghomashchi, S. Shabestari, J. Hejazi, Microstructural analysis of interfacial reaction between molten aluminum and solid iron, J. Mater. Process. Technol. 124 (2002) 345–352.
[31] A. Bouayad, C. Gerometta, A. Belkebir, A. Ambari, Kinetic interactions between solid iron and molten aluminium, Mater. Sci. Eng. A 363 (2003) 53–61.
[32] J.L. Song, S.B. Lin, S.B. Yang, C.L. Fan, Effects of Si additions on intermetallic compound layer of aluminum-steel TIG welding-brazing joint, J. Alloys Compd. 488 (2009) 217–222.
[33] F.C. Yin, M.X. Zhao, Y.X. Liu, Effect of Si on growth kinetics of intermetallic compounds during reaction between solid iron and molten aluminum, Trans. Nonferrous Metals Soc. China 23 (2013) 556–561.
[34] S.H. Chen, L.Q. Li, Y.B. Chen, J.M. Dai, J.H. Huang, Improving interfacial reaction nonhomogeneity during laser welding-brazing aluminum to titanium, Mater. Des. 32 (2011) 4408–4416.
[35] A. Szczepaniak, J. Fan, A. Kostka, D. Raabe, On the correlation between thermal cycle and formation of intermetallic phases at the interface of laser-welded aluminum-steel overlap joints, Adv. Eng. Mater. 14 (2012) 464–472.
[36] K. Bouche, F. Barbier, A. Coulet, Intermetallic compound layer growth between solid iron and molten aluminum, Mater. Sci. Eng. A 249 (1998) 167–175.
[37] S. Bozzi, A.L. Helbert-Etter, T. Baudin, B. Criqui, J.G. Kerbiguet, Intermetallic compounds in Al 6016/IF-steel friction stir spot welds, Mater. Sci. Eng. A 527 (2010) 4505–4509.
[38] T. Heumann, S. Dittrich, Uber die kinetik der reaktion von festem und flussigem aluminium mit eisen, Z. Met. 50 (1959) 617–625.
[39] G. Eggeler, W. Auer, H. Kaesche, Reactions between low alloyed steel and initially pure as well as iron-saturated aluminium melts between 670 and 800 degree, Z. Met. 77 (1986) 239–244.
[40] T. Kato, K. Nunome, K. Kaneko, H. Saka, Formation of the ζ phase at an interface between an Fe substrate and a molten 0.2 mass% Al–Zn during galvannealing, Acta Mater. 48 (2000) 2257–2262.
[41] R. Borrisutthekul, T. Yachi, Y. Miyashita, Y. Mutoh, Suppression of intermetallic reaction layer formation by controlling heat flow in dissimilar joining of steel and aluminum alloy, Mater. Sci. Eng. A 467 (2007) 108–113.
[42] M. Sonia, G. Supriyo, W. Stewart, M. Norman, Effect of laser processing parameters on the formation of intermetallic compounds in Fe–Al dissimilar welding, J. Mater. Eng. Perform. 23 (2014) 3361–3370.
[43] S. Kobayashi, T. Yakou, Control of intermetallic compound layers at interface between steel and aluminum by diffusion-treatment, Mater. Sci. Eng. A 338 (2002) 44–53.